



Visible light-excitable ZnO/2D graphitic-C₃N₄ heterostructure for the photodegradation of naphthalene

N. Mukwevho^a, N. Kumar^b, E. Fosso-Kankeu^{a,*}, F. Waanders^{a,c}, J. Bunt^c, S.S. Ray^{b,d}

^aWater Pollution Monitoring and Remediation Initiatives Research Group, Centre of Excellence in carbon based fuels, School of Chemical and Minerals Engineering, North West University, P. Bag X6001 Potchefstroom 2520, South Africa, emails: Elvis.FossoKankeu@nwu.ac.za/elvisfosso.ef@gmail.com (E. Fosso-Kankeu)

^bDST/CSIR National Centre for Nanostructured Materials, Council for Scientific and Industrial Research, Pretoria 0001, South Africa

^cCoal Research Group, Centre of Excellence in carbon based fuels, School of Chemical and Minerals Engineering, North West University, P. Bag X6001 Potchefstroom 2520, South Africa

^dDepartment of Applied Chemistry, University of Johannesburg, Doornfontein 2028, South Africa

Received 6 January 2019; Accepted 14 May 2019

ABSTRACT

In this study, ZnO/g-C₃N₄ heterostructure was synthesized with enhanced photodegradation potential for polycyclic aromatic hydrocarbons (PAHs) (viz. naphthalene) in water using visible light. The as-prepared catalysts were characterized via different techniques such as scanning electron microscopy, high-resolution transmission electron microscopy, fourier transform infrared, ultraviolet visible (UV-Vis), photoluminescence, and X-ray diffractometry to elucidate their physicochemical and structural properties. The identified properties of the newly synthesized heterostructure catalyst indicated a successful integration of physicochemical characteristics suitable for effective photocatalytic degradation activities. The kinetics study and mechanism of photodegradation of naphthalene using ZnO/g-C₃N₄ heterostructure have been discussed in detail. The photodegradation outcomes demonstrated that the synthesized heterostructure of semiconductors was more effective than the parent catalyst ZnO nanoparticles because of better light absorption for higher photogeneration of electrons and holes, suppressed recombination rate, and consequently prolonged availability of active species for degradation. The ZnO/g-C₃N₄ heterostructure has exhibited a photocatalytic efficiency of 84.5% in 4 h, which was relatively higher than the photocatalytic efficiency of individual photocatalysts. Thus, this report highlights the potential of as-prepared heterostructure for the photodegradation of naphthalene under visible light, therefore suggesting an avenue for the treatment of wastewater contaminated with PAHs.

Keywords: Zinc oxide; g-C₃N₄; Photocatalysts; Water pollution; PAHs; Naphthalene

1. Introduction

With continuous rising rate in population and progressive economy, environmental pollution with various toxic agents and industrial effluents constitutes a pressing challenge for the global environmental crisis. Coal is still one of the richest and central sources of global energy with the utilization of non-renewable energy sources consequently prompting

toxic discharges that are hazardous to the human environment. Amid coal ignition, fast pyrolytic responses in fuel-rich section result in the burning of coal particle that can consequently produce tar [1]. Hydrolysis of tar results into discharges of polycyclic aromatic hydrocarbons (PAHs) [2] into environment directly or indirectly. PAHs are introduced in water resources via anthropogenic and natural practices such as oil spill, seepage, burning of trash, wood, tobacco,

* Corresponding author.

and products of partial combustion of coal fuels. PAHs are synthetic toxins with at least two benzene rings fused together [3]. The simplest compound of PAHs is naphthalene ($C_{10}H_8$) which is one among the main hazardous waste products of coal and petroleum factories. It has been released into effluent streams of these factories due to high solubility in water. Their toxic, possible carcinogenic and mutagenic behaviour have harmful effects on human health as well as chronic and acute effects on animals and plants [4–6]. One of the most common diseases caused by naphthalene is hemolytic anaemia in children [7]. Thus, removal and fast degradation of naphthalene into less harmful products are of necessitated urgency.

Several methods have been utilized for the segregation of organic contaminants from the aqueous solution; however, they are not versatile to remove contaminants completely from wastewater [8–12]. Many purification methods are not appropriate as they produce huge sludge; require a great deal of energy to sustain high pressure and proper maintenance [13–21]. Photodegradation is an effective technique for the degradation of PAHs because it is quick, economical and environmentally friendly; furthermore, the use of solar energy is inexhaustible [10,22]. Recently, an extensive number of semiconductor nanomaterials (viz. SnO_2 , TiO_2 , $h-MoO_3$, ZnO, and their composites) have been considered as vital photocatalysts for the removal of harmful contaminants [9,23–25]. After TiO_2 , ZnO is the most explored metal oxide semiconductor because of its good catalytic, electronic, photochemical properties, and high quantum efficiency beside its cost-effective and non-toxic nature [24]. ZnO is also reported in the literature [26] as having the capacity to absorb over a higher section of the solar spectrum than TiO_2 . The ZnO nanostructures have high catalytic activity in the ultraviolet region and have ordinary performance in the visible light region. This has encouraged scientists to fabricate new hybrid materials with decreased band gap energy for improving the reaction with the sufficiently available visible light photons [27].

As of late, the two dimensional (2D) graphitic carbon nitride ($g-C_3N_4$) has received quite an attention in the arena of photocatalysis. The $g-C_3N_4$ exhibits photocatalytic property for the removal of organic effluents in the presence of visible light. Although the catalytic ability of $g-C_3N_4$ is still restricted because of the fast recombination rate [28], several methodologies such as doping with transition metals, loading known photocatalyst on the surface of a $g-C_3N_4$ and formation of nanohybrids, have been utilized to augment the photocatalytic performance of $g-C_3N_4$ [28,29]. Combining ZnO with $g-C_3N_4$ could yield a perfect heterostructure due to complementary overlapping band structures [30]. On irradiating light, the ground state electron get excited to transfer from the valence band (VB) of $g-C_3N_4$ to the conduction band (CB), later electron jump to the CB of ZnO [27,31] which results in better separation of photogenerated electron-hole for photocatalytic activity. Many reports have demonstrated the combination of ZnO nanoparticles (NPs) with other nanomaterials for the removal of dyes from water and revealed a high catalytic efficiency. However, to the best of our insight, no report has so far published about the utilization of ZnO/ $g-C_3N_4$ heterostructure for the photodegradation of naphthalene in the presence of visible light. In this study, ZnO NPs and its semiconductor heterostructure

with $g-C_3N_4$ NSs were synthesized by mechano-chemical and co-precipitation approaches, respectively, and later calcined at high temperature. The successful preparation of various catalysts was confirmed by various characterization techniques and used for the photodegradation of naphthalene in the presence of visible light. Insights of the photocatalytic mechanism were also illustrated for the degradation of naphthalene using ZnO/ $g-C_3N_4$ heterostructure.

2. Experimental

2.1. Chemicals

Melamine ($C_3H_6N_6$, 99%) and zinc acetate dehydrate ($Zn(Ac)_2 \cdot 2H_2O$, $\geq 98\%$) were received from Merck, South Africa. Naphthalene ($C_{10}H_8$, 99%) was obtained from Sigma-Aldrich, South Africa. The deionized water was utilized for naphthalene solution preparation and synthesis experiments.

2.2. Preparation of ZnO/ $g-C_3N_4$ heterostructure

Zinc acetate dihydrate was used for the preparation of ZnO NPs. 3.5 g zinc acetate dihydrate was ground in mortar for 1 h, then it was transferred in a crucible and heated at $350^\circ C$ for 4 h in a muffle furnace. The $g-C_3N_4$ nanosheets were synthesized by following two steps, first 5.5 g of melamine was heated in a covered crucible at low temperature ($80^\circ C$) and second, it was heated in a crucible at $550^\circ C$ for 4 h in a muffle furnace. The obtained sample was powdered and ultrasonicated in deionized water for 2 h. This solution was then centrifuged to eliminate the exfoliated $g-C_3N_4$. Moreover, ZnO/ $g-C_3N_4$ heterostructure was synthesized using zinc acetate dihydrate and melamine as precursors. In this experiment, 0.125 g of zinc acetate dihydrate was added in deionized water (20 mL) and stirred for 10 min. Then, 10.0 g of melamine was mixed in the previous solution and allowed to stir for 1.5 h. Subsequently, the mixture was introduced in the oven at $80^\circ C$ for 4 h. The final solution was then transferred in a covered crucible and heated at $500^\circ C$ for 3 h in a furnace.

2.3. Characterization of prepared samples

The size and morphological characteristics of the as-synthesized materials were determined by an Auriga FEG-SEM (Carl Zeiss, Germany), equipped with EDS and high-resolution transmission electron microscopy (HRTEM) (JEM-2100, JEOL, Japan), operated at 200 kV. The X-ray diffractometry (XRD) patterns were obtained using X-ray diffractometer of Philips PANalytical X'Pert pro pw 3040/60 (Netherlands) using a $Cu K\alpha$, $\lambda = 0.154$ nm radiation source with a 2θ range of 4° – 90° . Ultraviolet visible (UV-Vis) absorbance data were collected on a LAMBDA 750 UV Spectrophotometer (PerkinElmer, USA). Fourier transform infrared (FTIR) spectra were taken on ATR (attenuated total reflectance)-FTIR Spectrum 100 (PerkinElmer, USA). Horiba Jobin-Yvon NanoLog spectrometer (Germany) was used to investigate the photoluminescence (PL) characteristics of as-prepared materials. XPS data were received using Kratos Axis Ultra device (Kratos, UK), which used monochromatic ($Al K\alpha$) as excitation source.

2.4. Photocatalytic experiments

Naphthalene was used as a model contaminant to determine the photocatalytic performance of as-synthesized photocatalysts. 20 mg/L of naphthalene aqueous solution (10% v/v ratio of acetone to water) was considered for all photocatalytic experiments. Prior to light illumination, specific photocatalyst dosage was transferred in 100 mL naphthalene solution and the mixture was allowed to reach adsorption-desorption equilibrium with continuous stirring for 30 min in dark. The 300 W Xe lamp with a UV cut-off glass filter ($\lambda > 420$ nm) was used for sample irradiation. For each reading, 3 mL of solutions were removed at the different time period, filtered via a 0.45 μm membrane and analysed spectrophotometrically at a wavelength of 275 nm (λ_{max}). The photocatalytic performance of naphthalene using as-prepared photocatalysts was then calculated using Eq. (1) [32]:

$$\text{Photodegradation efficiency (\%)} = \left(\frac{C_0 - C_t}{C_0} \right) \times 100 \quad (1)$$

where C_0 represents the original naphthalene concentration, and C_t represents the naphthalene concentration at the time, t .

3. Results and discussions

Fig. 1 shows the XRD plots of the pure ZnO NPs, $\text{g-C}_3\text{N}_4$ NSs, and $\text{ZnO/g-C}_3\text{N}_4$ heterostructure. The outcomes reveal that all samples are crystalline in nature. The observed peaks of ZnO NPs and $\text{g-C}_3\text{N}_4$ NSs are well matched with JCPDS No. 36-1451 and JCPDS No. 87-1526, respectively [24,27]. For the $\text{ZnO/g-C}_3\text{N}_4$ heterostructure, there is no significant difference in the diffraction positions which indicates that the addition of $\text{g-C}_3\text{N}_4$ did not alter the growth of ZnO NPs. The peaks centred at 13.16° and 27.34° are related to crystal planes of (100) and (002) of $\text{g-C}_3\text{N}_4$ [27]. The XRD pattern of as-prepared $\text{ZnO/g-C}_3\text{N}_4$ heterostructure material exhibits both ZnO and $\text{g-C}_3\text{N}_4$ phases. For $\text{ZnO/g-C}_3\text{N}_4$ heterostructure, the melamine was used as a precursor for $\text{g-C}_3\text{N}_4$, whereas zinc acetate was used as a precursor for the ZnO. During the solution suspension and heating process, the melamine particles might adsorb on the surface of formed Zn(OH)_2 nanocrystals and later converted into a $\text{ZnO/g-C}_3\text{N}_4$ heterostructure upon calcination at high temperature.

The chemical composition and chemical bond characteristics of $\text{ZnO/g-C}_3\text{N}_4$ heterostructure can be explained by X-ray photoelectron spectroscopy (XPS). XPS survey scan of $\text{ZnO/g-C}_3\text{N}_4$ displayed in Fig. S1. The noticeable peaks in survey scan were related to C, N, O, and Zn. As seen in Fig. 2a, Zn 2p XPS scan exhibited doublet peaks of Zn 2p $^{1/2}$ and Zn 2p $^{3/2}$ at 1,044.5 and 1,021.4 eV, respectively, which could be ascribed to Zn $^{2+}$ oxidation state of ZnO in $\text{ZnO/g-C}_3\text{N}_4$ heterostructure [33]. The high resolution spectrum of O 1s (Fig. 2b) demonstrated three peaks at 529.7, 531.4, and 533.4 eV corresponding to Zn–O, C–O/O–H, and C=O respectively. Fig. 2c depicts the C 1s spectrum which was deconvoluted into three peaks. The peaks located at 284.6 and 286.0 eV were assigned to C–C and C–O, respectively, whereas higher energy peaks (287.9 eV) were attributed to C–N–C coordination in the C_3N_4 lattice [34].

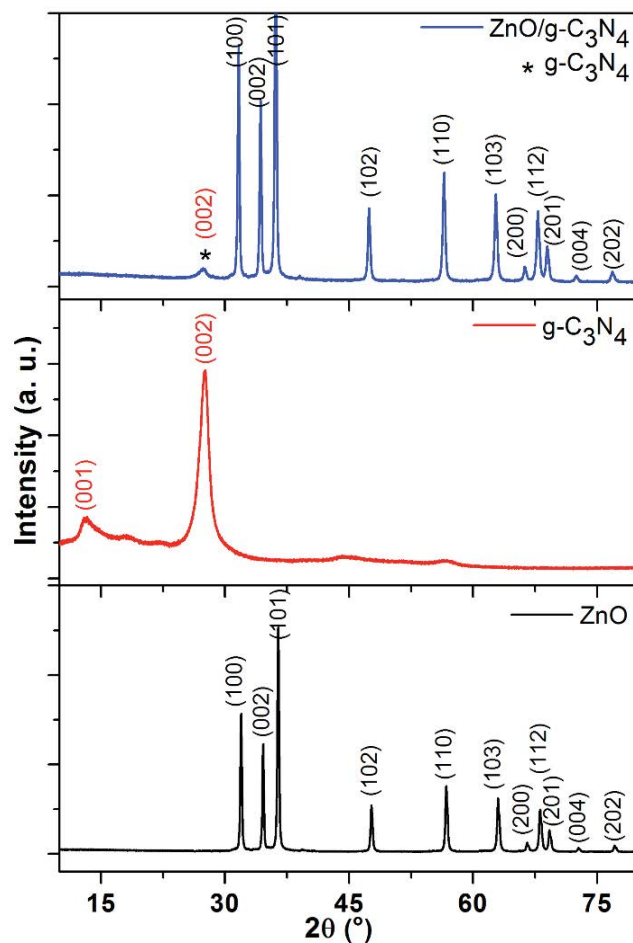


Fig. 1. XRD pattern of ZnO NPs, $\text{g-C}_3\text{N}_4$ NSs and $\text{ZnO/g-C}_3\text{N}_4$ heterostructure.

In N 1s spectrum in Fig. 2d, asymmetric peak could be deconvoluted into three Gaussian peaks. The N 1s peaks centred at 398.8 eV can be ascribed to sp^2 -hybridized N (C=N–C). The higher energy peaks at 399.4 and 400.3 eV were attributed to N–(C) $_3$ (tertiary nitrogen) and $-\text{NH}_x$, respectively [34].

The overall morphological features of the as-synthesized ZnO NPs, $\text{g-C}_3\text{N}_4$ NSs, and $\text{ZnO/g-C}_3\text{N}_4$ heterostructure are represented in Fig. 3. ZnO crystals have shown the mixed morphologies of nanorods and spherical like structures but have dominance of spherical structures. The evolution of these morphologies might occur due to escaping of CO_2 from the zinc acetate powder on heating. In the $\text{g-C}_3\text{N}_4$ case, a 2D layered morphology with varied thickness was noticed (Fig. 3b). These sheets are fluffy and contain clearly visible porous layers. This can be accredited to step-wise synthesis of $\text{g-C}_3\text{N}_4$ involving melem (intermediate stage) formation and condensation with the evolution of NH_3 [35]. Moreover, the morphological feature of the $\text{ZnO/g-C}_3\text{N}_4$ heterostructure is dissimilar from pure $\text{g-C}_3\text{N}_4$ and ZnO. ZnO NPs are anchored over the surface of the $\text{g-C}_3\text{N}_4$ NSs in the $\text{ZnO/g-C}_3\text{N}_4$ heterostructure. It was observed that sphere-like structures were more common than rod-like structures on the nanosheets (Fig. 3d). This possibly occurred as the heterostructure proceeded, using a co-precipitation method in which Zn(OH)_4^{2-} growth units were stabilized

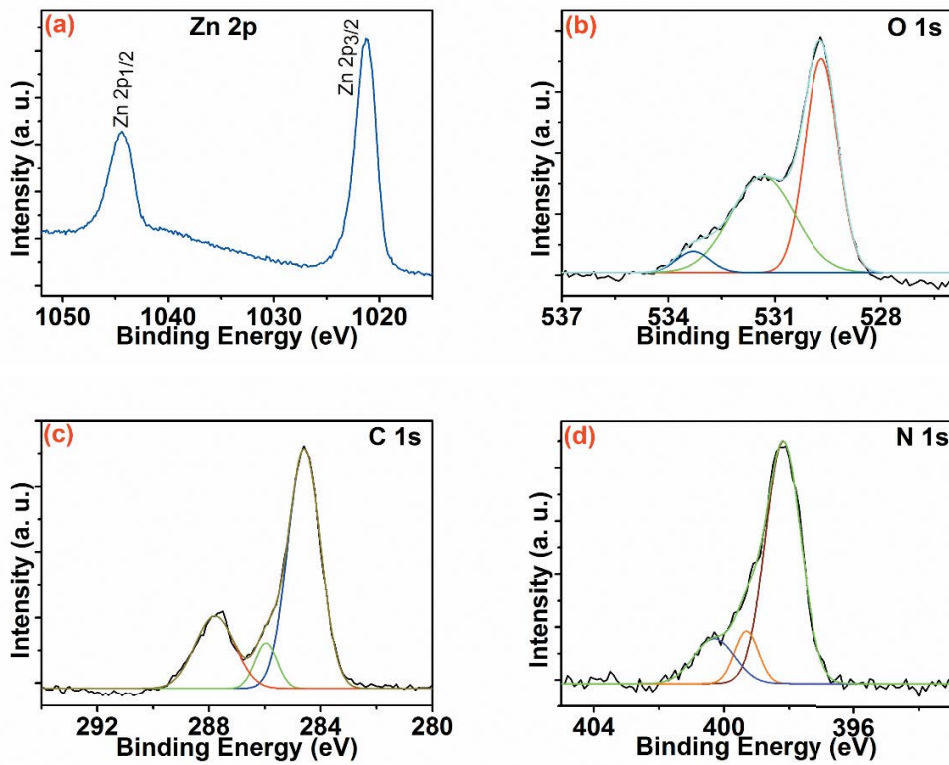


Fig. 2. XPS spectra of ZnO/g-C₃N₄: (a) Zn 2p, (b) O 1s, (c) C 1s and (d) N 1s.

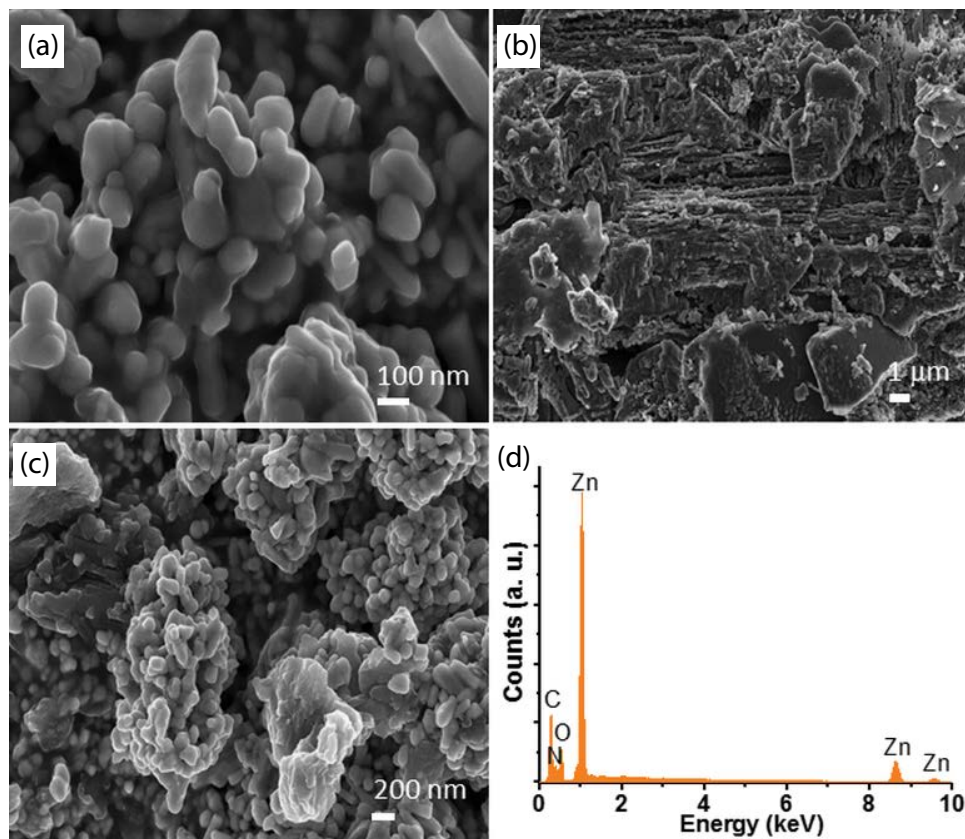


Fig. 3. SEM images of (a) ZnO NPs, (b) g-C₃N₄ NSs, and (c) ZnO/g-C₃N₄ heterostructure; EDS spectrum of the ZnO/g-C₃N₄ heterostructure (d).

by acetate ligands (from zinc precursor) and amine groups (from melamine) [24]. It has depressed the straightforward growth of ZnO and results in more spherical particles. Besides, some nanorod-like structures were noticed due to the coalescence of spherical particles at high temperature conditions. The elemental distribution of the ZnO/g-C₃N₄ heterostructure is explained by the EDS spectrum depicted in Fig. 3d. Carbon (C), oxygen (O), nitrogen (N), and zinc (Zn) could be observed in the EDS spectrum of the heterostructure, and confirming the as-synthesized samples are of high purity. Atomic ratio of elemental composition of ZnO/g-C₃N₄ heterostructure has been listed in Table S1. In addition, the interior morphological features of the ZnO/g-C₃N₄ heterostructure were observed by TEM and HRTEM images (Figs. 4a and b). It can be perceived that spherical particles of ZnO are implanted in the 2D lamellar structure of g-C₃N₄. Fig. 4c shows the lattice fringe ($d = 0.336$ nm) which relates to the (002) plane direction of g-C₃N₄ crystals, whereas the lattice fringe ($d = 0.261$ nm) in Fig. 4d relates to the (002) plane direction of the ZnO crystals [31,36]. HRTEM observations are well matched with XRD results and confirm the successful development of ZnO/g-C₃N₄ heterostructure. These outcomes show the construction of hetero-junction between g-C₃N₄ and ZnO, which would result in a better parting of photo-generated holes and electrons.

Fig. 5 exhibits the absorbance characteristics of the photocatalysts, which were observed by UV-vis spectroscopy. The absorption edges of the ZnO/g-C₃N₄ heterostructure move to higher wavelengths in comparison to ZnO NPs. This clearly indicates that the absorption edges of ZnO/g-C₃N₄ heterostructure photocatalyst move to the lower energy spectrum (Fig. 5). The band gap of the photocatalysts was calculated via Tauc's plot using a UV-vis absorption spectrum. Tauc's plot could be obtained by the following expression [32]:

$$(\alpha h\nu) = A(h\nu - E_g)^{\frac{1}{2}} \quad (2)$$

where α , ν , h and A stand for the absorption coefficient, frequency, Planck constant, and a constant, respectively. E_g represents the band gap energy. The Tauc's graph of $(\alpha h\nu)^2$ vs. $(h\nu)$ for ZnO NPs, g-C₃N₄ NSs and ZnO/g-C₃N₄ heterostructure is displayed in Figs. 5b–d. The approximate

values of the band gap energy would be determined by extra-plotting the tangent intercept to the x -axis in the Tauc's plot [32,37]. The band gap of ZnO NPs and g-C₃N₄ NSs was found to be 3.32 and 2.69 eV, respectively, but the band gap energy of the ZnO/g-C₃N₄ heterostructure decreased to 2.90 eV. It indicates that the construction of tightening chemically bonded interface between the g-C₃N₄ and ZnO could make a ZnO/g-C₃N₄ heterostructure move to the lower energy spectrum. The overall absorption spectrum for the ZnO/g-C₃N₄ heterostructure was better than the rest of the two samples. Considerably, the ZnO/g-C₃N₄ heterostructure should exhibit better photocatalytic activity towards naphthalene degradation.

The representative functional bands in the FTIR spectrum are alike to those of bulk materials (Fig. 6). The peaks in the range of 3,300–3 000 cm⁻¹ are related to primary and secondary amine groups of g-C₃N₄ NSs, and their H-bonding (intermolecular) interactions. Several peaks in the region of 1,700–900 cm⁻¹ are accredited to the vibration peaks of heterocyclic aromatic CN comprising either partial condensation (connecting C–NH–C units) or full condensation (trigonal N(–C)₃), corroborating the presence of stretched nets of C–N–C bonds. The peaks at 1,621; 1,318; and 1,240–1,590 cm⁻¹ could be precisely ascribed to C=N stretching, C–N stretching and C–N heterocyclic stretching, respectively [9,38,39]. A characteristic peak at 799 cm⁻¹ belongs to a breathing mode of the tris-triazine units. For the ZnO/g-C₃N₄ heterostructure, all typical vibrational peaks of g-C₃N₄ NSs were noticed with a slight shift in peak value and comparatively decreased intensity. The peaks at 2,956 and 2,924 cm⁻¹ relates to asymmetric and symmetric stretching of aliphatic methylene (–C–H) [39]. A low-intensity peak at 1,727 cm⁻¹ is obtained from the carboxyl (–C=O) group of acetate. These peaks appeared due to the presence of acetate residue on the exterior of ZnO NPs. Thus, based on the FTIR and XRD results, the occurrence of both ZnO NPs and g-C₃N₄ NSs in the heterostructure is confirmed.

The PL spectra were investigated to reveal the invisible agents (viz. defects and surface/trap states) and recombination, transfer and migration routes of photo-excited charge carriers in the photocatalyst [32]. The recombination of electron and holes emit the PL emission spectrum. The low intensity of the emission spectrum suggests a less probability

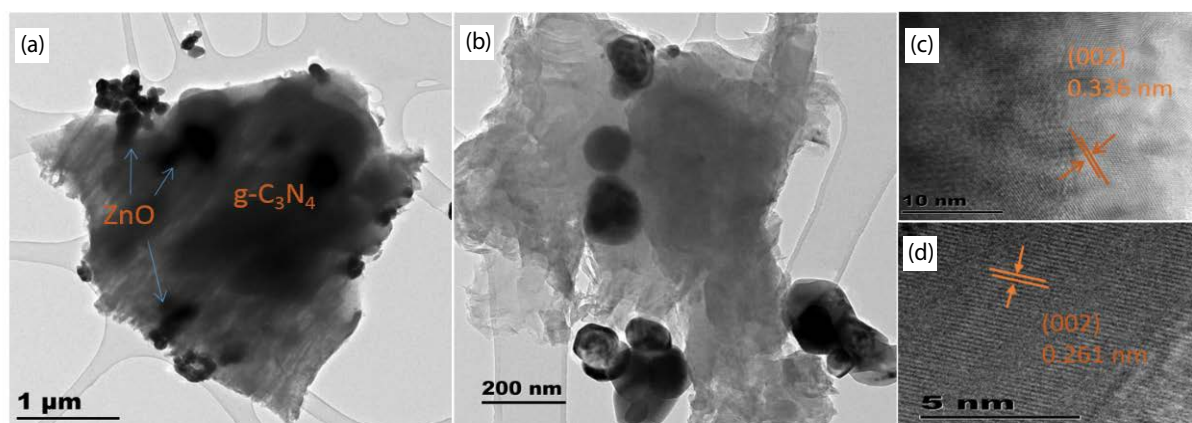


Fig. 4. (a–b) TEM images and (c–d) HRTEM images of the ZnO/g-C₃N₄ heterostructure.

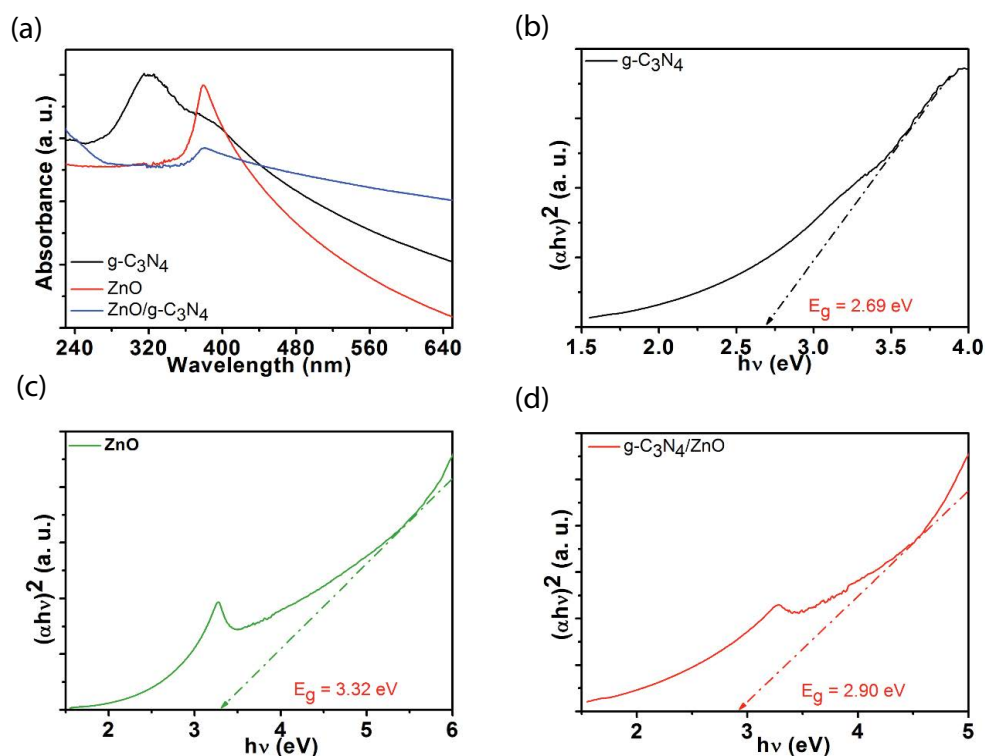


Fig. 5. (a) UV-Vis spectra of ZnO NPs, g-C₃N₄ NSs and ZnO/g-C₃N₄ heterostructure; Tauc's plot for g-C₃N₄ NSs (b), ZnO NPs (c), and ZnO/g-C₃N₄ heterostructure (d).

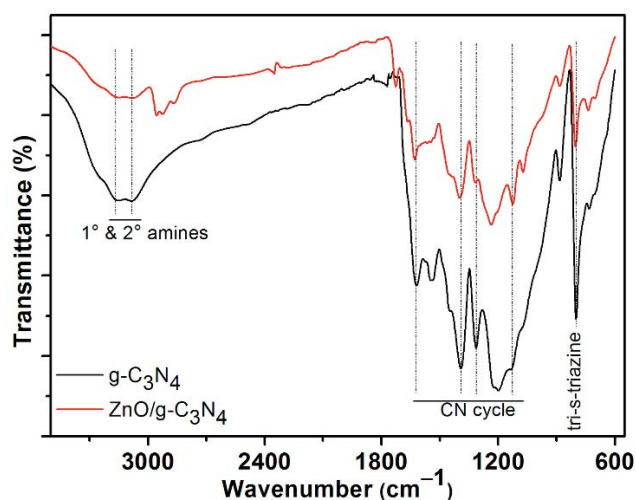


Fig. 6. FTIR spectra of g-C₃N₄ NSs and ZnO/g-C₃N₄ heterostructure.

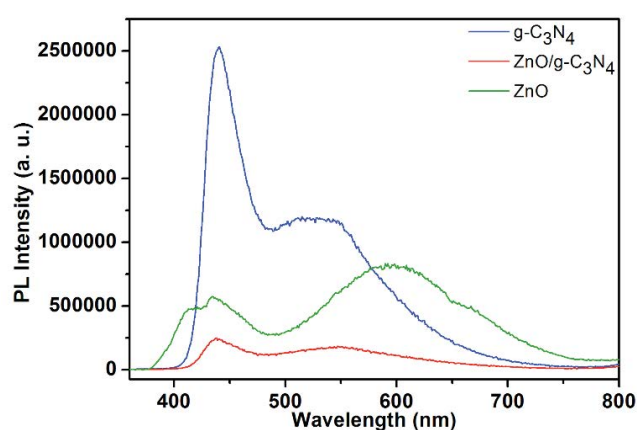


Fig. 7. PL spectra of ZnO NPs, g-C₃N₄ NSs, and ZnO/g-C₃N₄ heterostructure.

of recombination of photogenerated electron–hole pairs. On contrary, a better PL emission spectrum indicates moderately high re-combination of photogenerated charge carriers. Fig. 7 displays the PL spectra of the nanomaterials at room temperature with an excitation wavelength of 350 nm. The PL spectrum of g-C₃N₄ NSs revealed two transition band at 440 nm and broad asymmetric band centred at ~514 nm. The first band corresponds to photo-induced electron transition between anti-bonding (σ^*) and lone pair (LP) electron states of nitrogen atoms. The second band is associated with the

transitions of electrons between antibonding (π^*) and LP states and antibonding (π^*) to bonding π states. For ZnO NPs, the PL spectrum consists of two asymmetric bands, the weak one with a shoulder in the blue region (maximum intensity at ~416 and ~434 nm) and a broadband in the green range (maximum intensity at ~591 nm) was detected. The first band emission from 408 to 438 nm can be ascribed to zinc interstitials (Zn_i) carrying different charges (0, 1+, and 2+) [40]. Emission in the region 448–465 nm can be assigned to zinc vacancies (V_{zn}) [41]. Emission peaks found in the region from 490–615 nm originated from single and doubly

charged oxygen vacancies (V_o^+ and V_o^{2+}) [42]. Emission in the orange-red region from 615–750 nm is assigned to oxygen interstitials (O_i) [42]. For ZnO/g- C_3N_4 heterostructure, the emission peak intensity significantly decreased in comparison with g- C_3N_4 NSs, showing lesser recombination of free charge carriers. Thus, the addition of ZnO NPs on the surface of g- C_3N_4 NSs might diminish the recombination of electron-hole pairs as ZnO NPs trapped the electrons from the CB of g- C_3N_4 NSs. Based on PL observation, ZnO/g- C_3N_4 heterostructure should be a better photocatalyst than both ZnO NPs and g- C_3N_4 NSs.

3.1. Photocatalytic performance

The photocatalytic performance of variously prepared photocatalysts for organic contaminant naphthalene was examined. As seen in Fig. 8a, the effect of a catalyst dose on the degradation efficiency of naphthalene was observed by varying the catalyst amount in 20 mg/L solution at pH 4 under visible light at 25°C for 2 h. These outcomes showed that the increment of catalyst dose from 25 to 100 mg increased the photodegradation efficiency of naphthalene. Therefore, the most effective photodegradation of naphthalene using ZnO NPs, g- C_3N_4 NSs, and ZnO/g- C_3N_4 heterostructure was achieved with a higher catalyst dose. The photolysis of naphthalene was performed under visible light without using a catalyst. It exhibited 7.2% degradation efficiency in visible light (shown as blank in Fig. 8a). Degradation experiments were also executed in the dark using a catalyst to check adsorption behaviour. There were no significant changes in the degradation efficiency of naphthalene in the

absence of light illumination, showing that the utilization of light is necessary to enhance the photodegradation of naphthalene. The ZnO NPs and ZnO/g- C_3N_4 heterostructure managed to degrade 74.2% and 84.5% of naphthalene after 4 h, respectively. Relatively lower photodegradation efficiency (60%) is noticed when using g- C_3N_4 NSs which is comparatively less than that attained by ZnO NPs and ZnO/g- C_3N_4 heterostructure. This proved that the amalgamation of the g- C_3N_4 catalyst upgraded the photocatalytic efficiency of ZnO NPs and possibly occurred due to better segregation of photogenerated e^-/h^+ pairs.

For the kinetic study, the effect of time on the photodegradation efficiency of naphthalene was carried out using optimized dose (100 mg) of photocatalyst and 100 mL naphthalene solution (20 mg/L, pH = 4) under visible light (Fig. 8b). It was noticed that the photodegradation activity increased with time. This occurred due to a reduced concentration of naphthalene in the solution via photocatalysis with time. No significant changes in the photodegradation were noticed in the absence of light and in the case where no catalyst was present, suggesting naphthalene stability in normal conditions. After the coupling of ZnO NPs, the photocatalytic stability of g- C_3N_4 NSs is enhanced, demonstrating that the immobilization of ZnO can delay the recombination of photogenerated e^-/h^+ pairs. Moreover, the photodegradation using ZnO/g- C_3N_4 heterostructure catalyst is evidently better than individual catalysts. This can be attributed to better absorption in the visible range as narrower band gap energy to yield a high number of the e^-/h^+ pairs and consequently more reactive oxygen species (ROS) for naphthalene degradation.

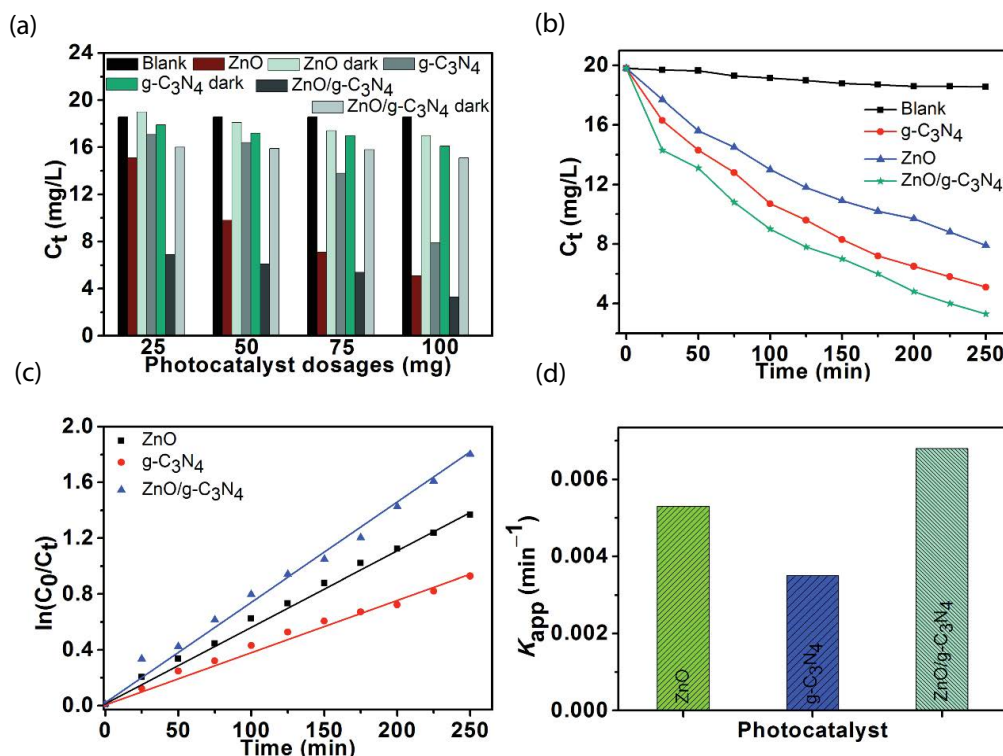


Fig. 8. Photocatalytic degradation of naphthalene: (a) catalyst dosages; (b) kinetic study; (c) kinetic relationship of $\ln(C/C_0)$ vs. time curve; (d) plot of kinetic rate constants.

Moreover, the photocatalytic degradation kinetics was further investigated via pseudo-first-order kinetics model, as displayed in Fig. 8c. The acquired experimental kinetics data matched well with the pseudo-first kinetics model which can be mathematically expressed as follows [9,32]:

$$\ln\left(\frac{C_0}{C_t}\right) = K_{app} t \quad (3)$$

where C_0 and C_t signify the concentration of naphthalene at time 0 and t , respectively, t represents the reaction time (min), K_{app} denotes the calculated apparent reaction rate constant (min^{-1}). A linear relation was noticed when a graph was plotted between $\ln(C_0/C_t)$ and t for the naphthalene degradation (Fig. 8c). Additionally, the apparent rate constant values for ZnO NPs, $g\text{-C}_3\text{N}_4$ NSs and ZnO/ $g\text{-C}_3\text{N}_4$ heterostructure were determined using a plot of $\ln(C_0/C_t)$ and t . A considerably high value of the apparent rate constant $0.0068 (\text{min}^{-1})$ obtained by the ZnO/ $g\text{-C}_3\text{N}_4$ heterostructure in comparison with ZnO NPs, $g\text{-C}_3\text{N}_4$ NSs, indicates the fast photodegradation of naphthalene using the heterostructure (Fig. 8d). These observations suggest that there might be a creation of the hetero-junction between ZnO NPs and $g\text{-C}_3\text{N}_4$ NSs, which provides better photocatalytic activity.

To understand the mechanistic pathways of charge separation and transfer, the CB and VB potential were calculated using the given mathematical equations [32,43]:

$$E_{VB} = \chi - E_e + 0.5E_g \quad (4)$$

$$E_{CB} = E_{VB} - E_g \quad (5)$$

where E_{CB} and E_{VB} signify the CB and VB potential, respectively, E_g represents the band gap energy, $E_e (=4.5 \text{ eV})$ represents the free electrons energy on the hydrogen scale. The χ is the absolute electronegativity of the material. It could be calculated via the geometric mean of the absolute electronegativity of atoms forming semiconductor materials. The related equation is expressed as follows [43]:

$$\chi = \left[x(A)^a x(B)^b \right]^{\frac{1}{(a+b)}} \quad (6)$$

where a and b represent the number of atoms present in the particular compound. In the case of $g\text{-C}_3\text{N}_4$, the calculated value of χ and E_g are 4.73 and 2.69 eV, respectively, whereas ZnO values are 5.74 and 3.32 eV, respectively [32,43]. Thus, E_{VB} and E_{CB} of $g\text{-C}_3\text{N}_4$ were estimated to be +1.57 eV/NHE and -1.15 eV/NHE, respectively. E_{VB} and E_{CB} of ZnO were determined to be +2.90 eV/NHE and -0.42 eV/NHE, respectively. Based on these values, a schematic presentation of a plausible mechanistic pathway of charge separation and transfer for the photodegradation of naphthalene using ZnO/ $g\text{-C}_3\text{N}_4$ hetero-junction under light illumination was constructed and is presented in Fig. 9.

ZnO NPs and $g\text{-C}_3\text{N}_4$ NSs can create an efficient hetero-junction arrangement due to the complementary overlying band energy structure. Electron-hole pairs are generated when the ZnO/ $g\text{-C}_3\text{N}_4$ heterostructure is irradiated with a particular light frequency ($h\nu \geq E_g$). The electrons in the CB of $g\text{-C}_3\text{N}_4$ NSs would move to CB of ZnO NPs due to higher energy levels for CB of $g\text{-C}_3\text{N}_4$. Herein, interfacial photo-generated charge carriers transfer can enhance the lifetime of e^-/h^+ pairs by quashing the recombination rate. These high numbers of separated electrons in CB of ZnO NPs could be utilized for reduction reactions, while holes present in the VB of $g\text{-C}_3\text{N}_4$ NSs would lead to oxidation reactions [27]. The accumulated photogenerated electrons on the CB take part in reaction with O_2 molecules adsorbed on the catalyst to yield anion oxygen radicals (O_2^-) as CB of ZnO has more negative potential (-0.42 eV/NHE) than the potential value of O_2/O_2^- ($E^0(\text{O}_2/\text{O}_2^-) = -0.33 \text{ eV/NHE}$) [27]. The adsorbed O_2 can also be converted into H_2O_2 in the presence of light and electrons because the CB energy levels of ZnO NPs and $g\text{-C}_3\text{N}_4$ NSs are more negative than $\text{O}_2/\text{H}_2\text{O}_2$ ($E^0(\text{O}_2/\text{H}_2\text{O}_2) = +0.682 \text{ eV/NHE}$) [43,44]. Furthermore, the formed H_2O_2 can get involved with electrons to provide hydroxyl radicals (OH^\bullet) whereas, the holes at VB of $g\text{-C}_3\text{N}_4$ NSs interacts directly with $\text{H}_2\text{O}/\text{OH}$ ions on the surface of ZnO/ $g\text{-C}_3\text{N}_4$ heterostructure

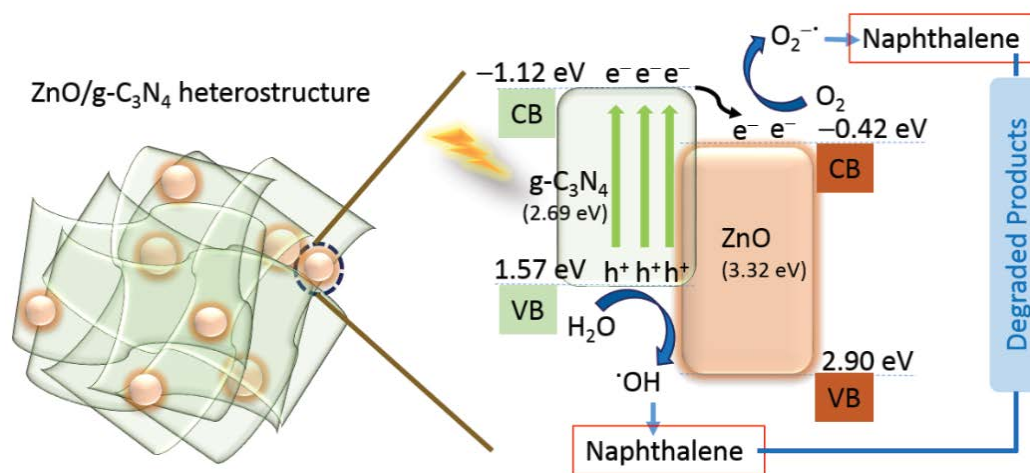
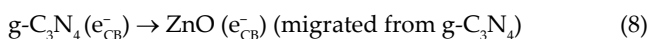
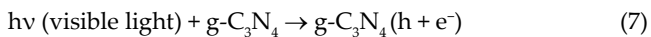


Fig. 9. Schematic presentation of a plausible mechanistic pathway of charge separation and transfer during photodegradation of naphthalene, using the synergistic effect of the ZnO/ $g\text{-C}_3\text{N}_4$ heterostructure under visible light.

to produce highly reactive hydroxyl radicals ($\cdot\text{OH}$). The role of as-produced ROS in the degradation of naphthalene can be described by the subsequent reactions:



The transfer of charge carriers (e^-/h^+) through the interfacial coupling of ZnO NPs and $\text{g-C}_3\text{N}_4$ NSs improved the photocatalytic performance of ZnO/ $\text{g-C}_3\text{N}_4$ heterostructure for naphthalene degradation due to suppression in the recombination of e^-/h^+ pairs. The photodegradation performance of studied nanomaterials for the degradation of naphthalene can be arranged in descending order trend as: ZnO/ $\text{g-C}_3\text{N}_4$ heterostructure > ZnO NPs > $\text{g-C}_3\text{N}_4$ NSs. This order can be supported by PL spectra, where the ZnO/ $\text{g-C}_3\text{N}_4$ heterostructure showed emission bands of lesser intensity, confirming a suppressed recombination rate of free electrons and holes which ultimately improved photocatalytic activity. Moreover, it may be accredited to the prolonged production of ROS (such as $\cdot\text{O}_2^-$, $\cdot\text{OH}$, and $\cdot\text{OOH}$) in the case of ZnO/ $\text{g-C}_3\text{N}_4$ heterostructure than bare ZnO NPs and $\text{g-C}_3\text{N}_4$ NSs. The band alignment yields an intimate contact surface between ZnO NPs and $\text{g-C}_3\text{N}_4$ NSs, which results in easier separation and distribution of photogenerated e^-/h^+ pairs. The recombination rate of e^-/h^+ pairs in bare $\text{g-C}_3\text{N}_4$ NSs is relatively fast, which outcomes in lower photocatalytic performance.

Furthermore, a comparative study of naphthalene photodegradation using various recently reported photocatalyst

with specific parameters such as the illumination source, concentration, degradation efficiency and study time period is shown in Table 1. As noticed from Table 1, previously designed photocatalysts mostly used UV light to degrade naphthalene, which is not easily available and appropriate for practical applications [47]. In this context, the as-prepared ZnO/ $\text{g-C}_3\text{N}_4$ heterostructure photocatalyst in this study is efficient and effective for degradation of naphthalene to less-harmful products because it is inexpensive and has exhibited a comparatively better degradation performance under visible light.

4. Conclusion

An effective catalyst system, ZnO/ $\text{g-C}_3\text{N}_4$ heterostructure, was successfully developed with an aim to increase the photocatalytic degradation of the toxic PAH pollutant, naphthalene in water, using visible light. The preparation of the desired photocatalysts was confirmed via various characterization tools. The investigation of various parameters during photocatalytic experiments such as catalyst dosages optimization, photolysis and degradation in dark conditions was carried out to establish best reaction conditions for the degradation of naphthalene under visible light. The ZnO/ $\text{g-C}_3\text{N}_4$ heterostructure has demonstrated a photocatalytic efficiency of 84.5% in 4 h, which was relatively higher than the photocatalytic efficiency of bare ZnO NPs and $\text{g-C}_3\text{N}_4$ NSs. It was ascribed to the prolonged production of active oxygen species (such as $\cdot\text{O}_2^-$, $\cdot\text{OH}$, and $\cdot\text{OOH}$) in the ZnO/ $\text{g-C}_3\text{N}_4$ heterostructure. The band alignment offers a close intimate surface between ZnO and $\text{g-C}_3\text{N}_4$, which results in easier separation and distribution of photogenerated e^-/h^+ pairs. The improved light absorption in the visible region to produce a high number of e^-/h^+ pairs, suppressed recombination rate and narrower band gap energy are also accountable for the better photodegradation. Furthermore, the developed cheap and efficient photocatalyst might be used for degradation of other emerging pollutants.

Acknowledgements

The authors would like to thank the Water Research Commission (WRC) and the North-West University in South Africa for financial support. The authors are also grateful to DST/CSIR National Centre for Nano-Structured Materials, South Africa for providing facilities for the characterization of materials. The authors thank Mr. Nico Lemmer at the North-West University for his contribution.

Table 1
Comparative study of photocatalytic degradation of naphthalene with reported photocatalysts

Photocatalyst	Naphthalene concentration (mg/L)	Light source	Degradation (%) in time	Reference
TiO ₂ suspensions	5	125 W mercury lamp	~68% in 25 min	[7]
Fe-ZnO/PVA nanofibers	40	16 W UV lamp	80% in 240 min	[45]
TiO ₂ nanofiber mats	25	12 W UV lamp	80% in 60 min	[46]
ZnO/ $\text{g-C}_3\text{N}_4$ heterostructure	20	300 W Xenon lamp	85.5% in 240 min	This work

References

- [1] E.B. Ledesma, M.A. Kalish, P.F. Nelson, M.J. Wornat, J.C. Mackie, Formation and fate of PAH during the pyrolysis and fuel-rich combustion of coal primary tar, *Fuel*, 79 (2000) 1801–1814.
- [2] H.I. Abdel-Shafy, M.S.M. Mansour, A review on polycyclic aromatic hydrocarbons: source, environmental impact, effect on human health and remediation, *Egypt. J. Pet.*, 25 (2016) 107–123.
- [3] K.-H. Kim, S.A. Jahan, E. Kabir, R.J.C. Brown, A review of airborne polycyclic aromatic hydrocarbons (PAHs) and their human health effects, *Environ. Int.*, 60 (2013) 71–80.
- [4] N.-D. Dat, M.B. Chang, Review on characteristics of PAHs in atmosphere, anthropogenic sources and control technologies, *Sci. Total Environ.*, 609 (2017) 682–693.
- [5] A.M. Mastral, M.S. Callén, A Review on Polycyclic Aromatic Hydrocarbon (PAH) Emissions from Energy Generation, *Environ. Sci. Technol.*, 34 (2000) 3051–3057.
- [6] N. Mukwehho, E. Fosso-Kankeu, F. Waanders, N. Kumar, S.S. Ray, X.Y. Mbianda, Photocatalytic activity of Gd₂O₂CO₃:ZnO-CuO nanocomposite used for the degradation of phenanthrene, *SN Appl. Sci.*, 1 (2018) 10.
- [7] A. Lair, C. Ferronato, J.-M. Chovelon, J.-M. Herrmann, Naphthalene degradation in water by heterogeneous photocatalysis: An investigation of the influence of inorganic anions, *J. Photochem. Photobiol., A*, 193 (2008) 193–203.
- [8] N. Kumar, L. Reddy, V. Parashar, J.C. Ngila, Controlled synthesis of microsheets of ZnAl layered double hydroxides hexagonal nanoplates for efficient removal of Cr(VI) ions and anionic dye from water, *J. Environ. Chem. Eng.*, 5 (2017) 1718–1731.
- [9] N. Kumar, H. Mittal, S.M. Alhassan, S.S. Ray, Bionanocomposite hydrogel for the adsorption of dye and reusability of generated waste for the photodegradation of ciprofloxacin: a demonstration of the circularity concept for water purification, *ACS Sustainable Chem. Eng.*, 6 (2018) 17011–17025.
- [10] M. Farhadian, P. Sangpour, G. Hosseinzadeh, Preparation and photocatalytic activity of WO₃-MWCNT nanocomposite for degradation of naphthalene under visible light irradiation, *RSC Adv.*, 6 (2016) 39063–39073.
- [11] S. Shin, O. Shardt, P.B. Warren, H.A. Stone, Membraneless water filtration using CO₂, *Nat. Commun.*, 8 (2017) 15181.
- [12] N. Kumar, H. Mittal, V. Parashar, S.S. Ray, J.C. Ngila, Efficient removal of rhodamine 6G dye from aqueous solution using nickel sulphide incorporated polyacrylamide grafted gum karaya bionanocomposite hydrogel, *RSC Adv.*, 6 (2016) 21929–21939.
- [13] A.G. Fane, R. Wang, M.X. Hu, Synthetic membranes for water purification: status and future, *Angew. Chem. Int. Ed.*, 54 (2015) 3368–3386.
- [14] A. Lee, J.W. Elam, S.B. Darling, Membrane materials for water purification: design, development, and application, *Environ. Sci. Water Res. Technol.*, 2 (2016) 17–42.
- [15] K. Eryuruk, U. Tezcan Un, U. Bakır Ogutveren, Electrochemical treatment of wastewaters from poultry slaughtering and processing by using iron electrodes, *J. Cleaner Prod.*, 172 (2018) 1089–1095.
- [16] B. Khemila, B. Merzouk, A. Chouder, R. Zidelkhir, J.-P. Leclerc, F. Lapique, Removal of a textile dye using photovoltaic electrocoagulation, *Sustainable Chem. Pharm.*, 7 (2018) 27–35.
- [17] E. Fosso-Kankeu, A.F. Mulaba-Bafubandi, B.B. Mamba, T.G. Barnard, Prediction of metal-adsorption behaviour in the remediation of water contamination using indigenous microorganisms, *J. Environ. Manage.*, 92 (2011) 2786–2793.
- [18] H. Mittal, E. Fosso-Kankeu, S.B. Mishra, A.K. Mishra, Biosorption potential of Gum ghatti-g-poly (acrylic acid) and susceptibility to biodegradation by *B. subtilis*, *Int. J. Biol. Macromol.*, 62 (2013) 370–378.
- [19] E. Fosso-Kankeu, H. Mittal, S.B. Mishra, A.K. Mishra, Gum ghatti and acrylic acid based biodegradable hydrogels for the effective adsorption of cationic dyes, *J. Ind. Eng. Chem.*, 22 (2015) 171–178.
- [20] E. Fosso-Kankeu, H. Mittal, F. Waanders, I.O. Ntwampe, S.S. Ray, Preparation and characterization of gum karaya hydrogel nanocomposite flocculant for metal ions removal from mine effluents, *Int. J. Environ. Sci. Technol.*, 13 (2016) 711–724.
- [21] E. Fosso-Kankeu, H. Mittal, F. Waanders, S.S. Ray, Thermodynamic properties and adsorption behaviour of hydrogel nanocomposites for cadmium removal from mine effluents, *J. Ind. Eng. Chem.*, 48 (2017) 151–161.
- [22] W. Zhang, X. Li, Q. Zhao, Y. Hou, Y. Shen, G. Chen, Uniform α -Fe₂O₃ nanotubes fabricated for adsorption and photocatalytic oxidation of naphthalene, *Mater. Chem. Phys.*, 129 (2011) 683–687.
- [23] E.H. Umukoro, N. Kumar, J.C. Ngila, O.A. Arotiba, Expanded graphite supported p-n MoS₂-SnO₂ heterojunction nanocomposite electrode for enhanced photo-electrocatalytic degradation of a pharmaceutical pollutant, *J. Electroanal. Chem.*, 827 (2018) 193–203.
- [24] N. Kumar, H. Mittal, L. Reddy, P. Nair, J.C. Ngila, V. Parashar, Morphogenesis of ZnO nanostructures: role of acetate (COOH⁻) and nitrate (NO₃⁻) ligand donors from zinc salt precursors in synthesis and morphology dependent photocatalytic properties, *RSC Adv.*, 5 (2015) 38801–38809.
- [25] O.M. Ama, N. Kumar, F.V. Adams, S.S. Ray, Efficient and cost-effective photoelectrochemical degradation of dyes in wastewater over an exfoliated graphite-MoO₃ nanocomposite electrode, *Electrocatalysis*, 9 (2018) 623–631.
- [26] M.A. Behnajady, N. Modirshahla, R. Hamzavi, Kinetic study on photocatalytic degradation of C.I. Acid Yellow 23 by ZnO photocatalyst, *J. Hazard. Mater.*, 133 (2006) 226–232.
- [27] J.-X. Sun, Y.-P. Yuan, L.-G. Qiu, X. Jiang, A.-J. Xie, Y.-H. Shen, J.-F. Zhu, Fabrication of composite photocatalyst g-C₃N₄-ZnO and enhancement of photocatalytic activity under visible light, *Dalton Trans.*, 41 (2012) 6756–6763.
- [28] W.-J. Ong, L.-L. Tan, Y.H. Ng, S.-T. Yong, S.-P. Chai, Graphitic carbon nitride (g-C₃N₄)-based photocatalysts for artificial photosynthesis and environmental remediation: are we a step closer to achieving sustainability?, *Chem. Rev.*, 116 (2016) 7159–7329.
- [29] J. Wen, J. Xie, X. Chen, X. Li, A review on g-C₃N₄-based photocatalysts, *Appl. Surf. Sci.*, 391 (2017) 72–123.
- [30] W.-K. Jo, N.C.S. Selvam, Enhanced visible light-driven photocatalytic performance of ZnO-g-C₃N₄ coupled with graphene oxide as a novel ternary nanocomposite, *J. Hazard. Mater.*, 299 (2015) 462–470.
- [31] W. Liu, M. Wang, C. Xu, S. Chen, Facile synthesis of g-C₃N₄/ZnO composite with enhanced visible light photooxidation and photoreduction properties, *Chem. Eng. J.*, 209 (2012) 386–393.
- [32] N. Kumar, S.S. Ray, J.C. Ngila, Ionic liquid-assisted synthesis of Ag/Ag₂Te nanocrystals via a hydrothermal route for enhanced photocatalytic performance, *New J. Chem.*, 41 (2017) 14618–14626.
- [33] H. Chen, L. Lin, Y. Li, R. Wang, Z. Gong, Y. Cui, Y. Li, Y. Liu, X. Zhao, W. Huang, Q. Fu, F. Yang, X. Bao, CO and H₂ activation over g-ZnO layers and w-ZnO(0001), *ACS Catal.*, 9 (2019) 1373–1382.
- [34] L. Ge, F. Zuo, J. Liu, Q. Ma, C. Wang, D. Sun, L. Bartels, P. Feng, Synthesis and efficient visible light photocatalytic hydrogen evolution of polymeric g-C₃N₄ coupled with CdS quantum dots, *J. Phys. Chem. C*, 116 (2012) 13708–13714.
- [35] S. Yu, R.D. Webster, Y. Zhou, X. Yan, Ultrathin g-C₃N₄ nanosheets with hexagonal CuS nanoplates as a novel composite photocatalyst under solar light irradiation for H₂ production, *Catal. Sci. Technol.*, 7 (2017) 2050–2056.
- [36] X. Huang, M.-G. Willinger, H. Fan, Z.-L. Xie, L. Wang, A. Klein-Hoffmann, F. Girgsdies, C.-S. Lee, X.-M. Meng, Single crystalline wurtzite ZnO/zinc blende ZnS coaxial heterojunctions and hollow zinc blende ZnS nanotubes: synthesis, structural characterization and optical properties, *Nanoscale*, 6 (2014) 8787–8795.
- [37] Y. Wang, J. Cheng, S. Yu, E.J. Alcocer, M. Shahid, Z. Wang, W. Pan, Synergistic effect of N-decorated and Mn²⁺ doped ZnO nanofibers with enhanced photocatalytic activity, *Sci. Rep.*, 6 (2016) 32711.
- [38] P. Xia, B. Zhu, B. Cheng, J. Yu, J. Xu, 2D/2D g-C₃N₄/MnO₂ nanocomposite as a direct Z-scheme photocatalyst for enhanced

- photocatalytic activity, *ACS Sustainable Chem. Eng.*, 6 (2018) 965–973.
- [39] B.P.A. George, N. Kumar, H. Abrahamse, S.S. Ray, Apoptotic efficacy of multifaceted biosynthesized silver nanoparticles on human adenocarcinoma cells, *Sci. Rep.*, 8 (2018) 14368.
- [40] V. Kumar, H.C. Swart, M. Gohain, V. Kumar, S. Som, B.C. Bezuindenhoudt, O.M. Ntwaeaborwa, Influence of ultrasonication times on the tunable colour emission of ZnO nanophosphors for lighting applications, *Ultrason. Sonochem.*, 21 (2014) 1549–1556.
- [41] P. Rai, J.-N. Jo, I.-H. Lee, Y.-T. Yu, Fabrication of flower-like ZnO microstructures from ZnO nanorods and their photoluminescence properties, *Mater. Chem. Phys.*, 124 (2010) 406–412.
- [42] B. Panigrahy, M. Aslam, D.S. Misra, M. Ghosh, D. Bahadur, Defect-related emissions and magnetization properties of ZnO nanorods, *Adv. Funct. Mater.*, 20 (2010) 1161–1165.
- [43] M. Mousavi, A. Habibi-Yangjeh, M. Abitorabi, Fabrication of novel magnetically separable nanocomposites using graphitic carbon nitride, silver phosphate and silver chloride and their applications in photocatalytic removal of different pollutants using visible-light irradiation, *J. Colloid Interface Sci.*, 480 (2016) 218–231.
- [44] S. Adhikari, D. Sarkar, G. Madras, Hierarchical design of CuS architectures for visible light photocatalysis of 4-chlorophenol, *ACS Omega*, 2 (2017) 4009–4021.
- [45] A.D. Sekar, H. Muthukumar, N.I. Chandrasekaran, M. Matheswaran, Photocatalytic degradation of naphthalene using calcined FeZnO/PVA nanofibers, *Chemosphere*, 205 (2018) 610–617.
- [46] K. Mondal, S. Bhattacharyya, A. Sharma, Photocatalytic degradation of naphthalene by electrospun mesoporous carbon-doped anatase TiO₂ nanofiber mats, *Ind. Eng. Chem. Res.*, 53 (2014) 18900–18909.
- [47] E. Fosso-Kankeu, A.K. Mishra, Photocatalytic Degradation and Adsorption Techniques Involving Nanomaterials for Biotoxins Removal from Drinking Water, Alexandru Grumezescu, Ed., *Water Purification*, Academic Press, Elsevier, Vol. 5, 2017, pp. 323–354.

Supplementary Information

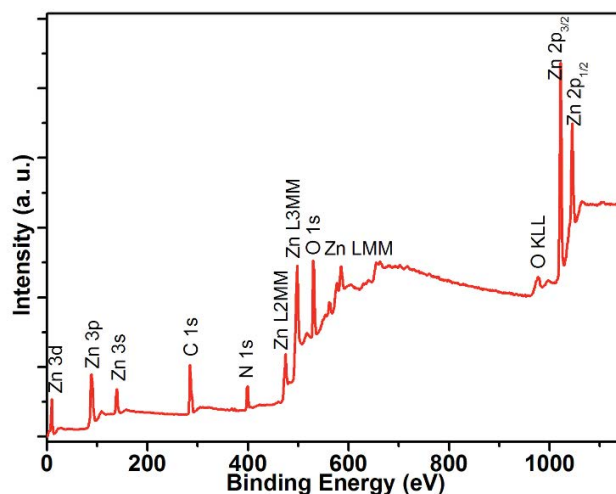


Fig. S1. XPS survey spectrum of ZnO/g-C₃N₄ heterostructure.

Table S1
Elemental quantification in ZnO/g-C₃N₄ heterostructure using XPS measurement

Element	Atomic (%)
C	45.8
O	27.1
Zn	15.6
N	11.5